Quantum Dots in an Amphiphilic Polyethyleneimine Derivative Platform for Cellular Labeling, Targeting, Gene Delivery, and Ratiometric Oxygen Sensing

Joonhyuck Park,[†] Junhwa Lee,[†] Jungheon Kwag,[‡] Yeonggyeong Baek,[‡] Bumju Kim,[§] Calvin Jinse Yoon,[⊥] Seoyeon Bok,[⊥] So-Hye Cho,[∥] Ki Hean Kim,[§,⊥] G-One Ahn,[⊥] and Sungjee Kim*[,†,‡]

[†]Department of Chemistry, [‡]School of Interdisciplinary Bioscience and Bioengineering, [§]Department of Mechanical Engineering, and [⊥]Division of Integrative Biosciences and Biotechnology, Pohang University of Science & Technology (POSTECH), San 31, Hyoja-Dong, Nam-Gu, Pohang, Gyeong-Buk 790-784, South Korea and [∥]Materials Architecturing Research Center, Korea Institute of Science and Technology, Hwarangno 14-gil 5, Seongbuk-gu, Seoul 136-791, South Korea

ABSTRACT Amphiphilic polyethyleneimine derivatives (amPEIs) were synthesized and used to encapsulate dozens of quantum dots (QDs). The QD—amPEI composite was ~100 nm in hydrodynamic diameter and had the slightly positive outer surface that suited well for cellular internalization. The QD—amPEI showed very efficient QD cellular labeling with the labeled cell fluorescence intensity more than 10 times higher than conventional techniques such as Lipofectamine-assisted QD delivery. QD—amPEI was optimal for maximal intracellular QD delivery by the large QD payload and the rapid endocytosis kinetics. QD—amPEI platform technology was demonstrated for gene delivery, cell-specific labeling, and ratiometric oxygen sensing. Our QD—amPEI platform has two partitions: positive outer surface and hydrophobic inside pocket. The outer positive surface was further exploited for gene delivery and targeting. Co-delivery of QDs and GFP silencing RNAs was successfully demonstrated by assembling siRNAs to the outer surfaces, which showed the transfection efficiency an order of magnitude higher than conventional gene transfections. Hyaluronic acids were tethered onto the QD—amPEI for cell-specific targeted labeling which showed the specific-to-nonspecific signal ratio over 100. The inside hydrophobic compartment was further applied for cohosting oxygen sensing phosphorescence Ru dyes along with QDs. The QD-Ru-amPEI oxygen probe showed accurate and reversible oxygen sensing capability by the ratiometric photoluminescence signals, which was successfully applied to cellular and spheroid models.

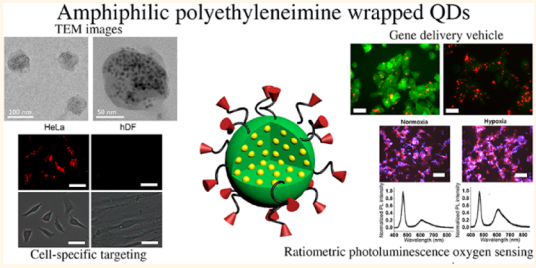

KEYWORDS: quantum dot · polyethyleneimine · cellular labeling · targeting · gene delivery · oxygen probe · amphiphilic encapsulation

Semiconductor nanocrystal quantum dots (QDs) have emerged as an alternative for fluorescence proteins or organic dyes in biological applications.[1] QDs have higher extinction coefficient and broader absorption range than organic fluorophores do and show high photostability and resistance against photobleaching. Highly crystalline QDs, prepared by solvothermal pyrolysis methods, have hydrophobic surface ligands, which need to be exchanged by foreign ligands or be encapsulated by amphiphilic macromolecules to apply them in aqueous phase.[2,3] The initial surface ligands of QDs are typically fatty acids such as oleic acid. Such fatty acids can be accumulated in adipocytes and also in nonadipocytes,[4] and for some QD applications such as cellular labeling, it may be optimal to deliver the QD with the initial fatty acid ligands.

Encapsulations of QDs using lipids or polymers have been reported by many groups. Lipid micelles or pegylated lipids have been used to encapsulate QDs.[5−7] Alkylated polymers were often used to transfer as-synthesized QDs to aqueous phase. Such polymers include poly(maleic anhydride-*alt*-tetradecene) (PMAT),[8] poly(methacrylate-*stat*-lauryl methacrylate),[9] PEG conjugated poly(maleic anhydride-*alt*-octadecene),[10] PEG conjugated triblock copolymers,[11] poly(styrene-*co*-maleic anhydride),[12] poly(acrylic acid) derivatized

* Address correspondence to sungjee@postech.ac.kr.

Received for review April 20, 2015 and accepted June 3, 2015.

Published online June 09, 2015
10.1021/acsnano.5b02357

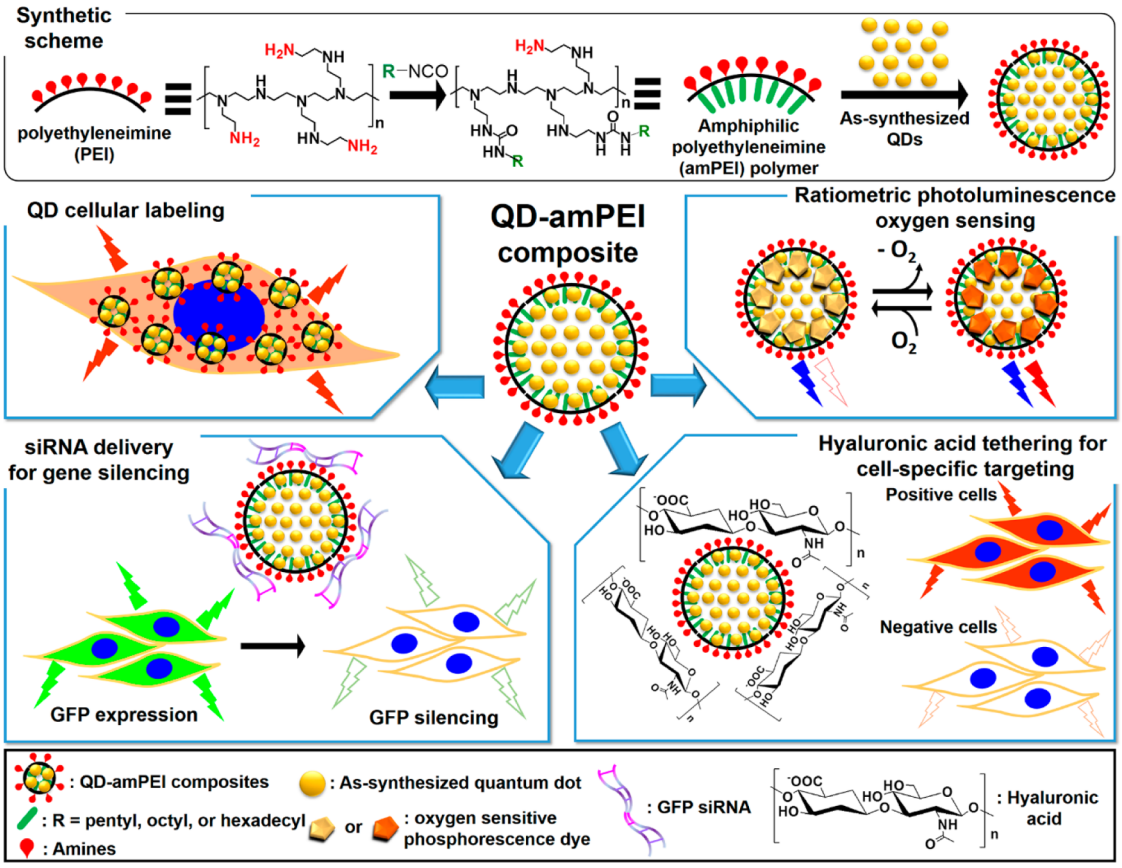

Scheme 1. Schematic representations for the synthesis of amphiphilic polyethyleneimine derivatized polymer (amPEI) and the encapsulation of dozens of QDs in amPEI for QD–amPEI composite preparation (top), and demonstrated QD–amPEI platform applications: QD cellular labeling, siRNA delivery for GFP gene silencing, hyaluronic acid tethering for cell-specific targeting, and ratiometric photoluminescence oxygen sensing (from upper left box to counterclockwise order).

amphiphilic polymers,[13,14] poly(isoprene-*block*-ethylene glycol),[15] and poly(aspartic acid-*grafted*-dodecylamine).[16] Most of these strategies are single individual QD encapsulation, which may be more suited for single particle imaging applications. For many other applications such as QD cellular labeling, QDs may be better to be packaged in dozens rather than single individual fashion. Conventional QD cellular labeling includes polymer-encapsulated QDs with cationic peptide coating (*i.e.*, Qtracker) and Lipofectamine-assisted delivery of negatively surface charged QDs. Hexadecyltrimethylammonium bromide (CTAB) encapsulated QDs can be also used; however, they typically show high cytotoxicity.[17]

For efficient QD cellular delivery, cationic amphiphilic delivery vehicles for dozens of QDs can be advantageous because most parts of cell membrane are slightly negatively charged in physiological condition and positive charged delivery vehicle can be more accessible. In terms of the size of delivery vehicle, amphiphilic delivery vehicle with inside hydrophobic core (where QDs can be loaded) of ~100 nm is expected to be optimal.[18−20] Xu and co-workers reported spherical hyperbranched polyethyleneimine (PEI) with 98 nm in hydrodynamic (HD) diameter to be most effective in delivering genes among PEIs sizes in the range 47−260 nm.[18] Single individual QDs or small QD vehicles which contain a smaller number of QDs inside may show rapid cellular internalization; however, the net QD labeling efficiency may not be optimal because of the small QD payload per vehicle. Large QD vehicles may show enhanced QD payloads but may suffer from slow intracellular uptake kinetics because the larger vehicle requires higher reorganization energy in membrane warping during the internalization. Such trade-offs have been observed in the case of NP intracellular accumulations by different sizes, where NP size ~60 nm was optimal.[19,20] We designed a QD platform which consists of cationic amphiphilic polymers of size ~100 nm. The QD packaging platform is designed to have a hydrophobic pocket which can contain dozens of as-synthesized QDs with fatty acids. We chose PEI as the polycationic polymer vehicle backbone and partially derivatized the PEIs with alkyl isocyanates to provide a controllable degree of amphiphilicity (Scheme 1). The QDs in amphiphilic PEI derivative polymer composites (QD–amPEIs) have as-synthesized QDs inside the hydrophobic pocket while exposing polycationic outer surfaces that can efficiently interact with cells. PEI has been widely studied for nonviral cationic vehicles for gene delivery.[21] Nann

used PEI to exchange original ligands of QDs and successfully dispersed the PEI-capped QDs in water showing the HD diameter of 10−20 nm.[22] Duan and co-workers reported PEG-conjugated, PEI-capped QDs penetrating cell membranes.[23] Alkylation of PEIs has been reported to tailor the gene delivery efficiency;[24] however, to the best of authors' knowledge, alkylated PEI has not been reported for QD encapsulations or for QD delivery vehicles.

We introduce QD−amPEI composite to demonstrate a QD platform that can be exploited for various applications which include cellular labeling, targeting, gene delivery, and ratiometric oxygen sensing (Scheme 1). The QD−amPEI showed very efficient QD cellular labeling with the labeled cell fluorescence intensity more than 10 times higher than the case of conventional QD cellular labeling techniques such as with Lipofectamine. The outer positive surface of QD−amPEI has been exploited for the gene delivery of siRNA and also for the conjugation of hyaluronic acid (HA) for cell-specific targeting. Our QD−amPEI platform also provides a hydrophobic pocket where dozens of QDs can equilibrate with hydrophobic molecular probes. The hydrophobic pocket acted as a unique partition co-accompanying QDs and oxygen indicating phosphorescence dyes for ratiometric photoluminescence(PL) sensing. The inner hydrophobic pocket allowed reversible interactions with microenvironment to monitor the local oxygen level, which was demonstrated in cellular and also in spheroid models.

RESULTS AND DISCUSSION

For amPEI, alkyl isocyanates were conjugated with PEI to form urea bonds. FT-IR measurements confirmed the urea bond by the vibration peaks at 1627 cm^{-1}, which corresponds to amide C═O stretching, and at 1544 cm^{-1}, which corresponds to amide N−H bending (see Supporting Information Figure S1). CdSe/CdS/ZnS (core/shell/shell) QDs, which fluoresce at 610 nm, were prepared by following modified successive ionic layer adsorption and reaction procedure (see Supporting Information for synthetic details. See Figure S2 for the absorption and emission spectra and Figure S3 for the TEM image). As-synthesized QDs were purified by precipitations by methanol and dispersed in chloroform. Typical QD samples showed the PL quantum efficiency (QE) higher than 60%. amPEI was dissolved in QD chloroform solution. MES buffer (pH 6.5, 100 mM) was added to the QD and amPEI mixture solution and the mixture was sonicated to transfer the QD−amPEIs to the aqueous phase. The chloroform was removed in vacuum. The typical QD−amPEI composites showed the HD diameter ∼100 nm and zeta potential ∼60 mV (see Supporting Information Figure S4a,b). TEM images of QD−amPEI showed the diameter around 100 nm, and the PL of QD−amPEI was almost identical to that of as-synthesized QDs (Figure 1a,b). Their colloidal

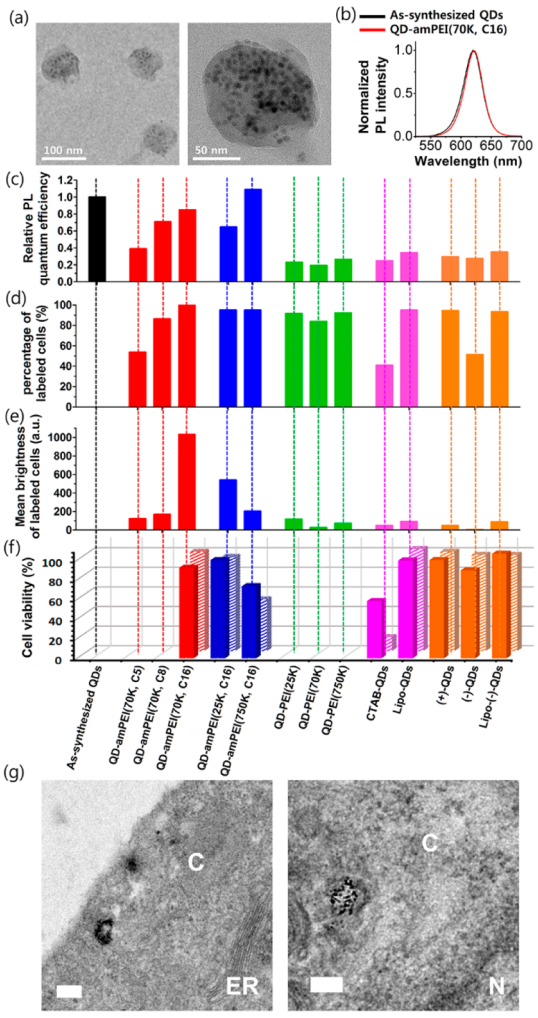

Figure 1. Characterization, intracellular delivering efficacy, and intracellular fate of QD−amPEI and other QD samples. (a) Transmission electron microscopy images of QD−amPEI-(70K, C16). (b) PL spectra of an as-synthesized QD sample and the QD−amPEI(70K, C16) composite sample prepared from the as-synthesized QDs. (c) Bar graphs showing relative PL intensities of QD−amPEI composite samples and other QD samples: as-synthesized QD sample, QD−amPEI(70K, C5), QD−amPEI(70K, C8), QD−amPEI(70K, C16), QD−amPEI(25K, C16), QD−amPEI(750K, C16), QD-PEI(25K), QD-PEI(70K), QD-PEI(750K), CTAB-QD, Lipo-QD, (+)-QD, (−)-QD, and Lipo-(−)-QD. All samples are dispersed in MES buffers except the as-synthesized QD sample which is dispersed in chloroform. (d) Bar graph showing the percentages of labeled HeLa cells (%) after co-incubations in serum-free media with the 13 QD samples in MES buffers. (e) Bar graphs showing the mean brightness values measured by flow cytometry for the labeled cells after the co-incubations with the 13 QD samples. (f) Bar graph showing the cell viabilities after the co-incubations with the QD−amPEI(70K, C16), QD−amPEI(25K, C16), QD−amPEI(750K, C16), CTAB-QD, Lipo-QD, (+)-QD, (−)-QD, and Lipo-(−)-QD samples for 12 h (solid bars) and for 48 h (bars with diagonal stripes). (g) Cross-sectional TEM images of HeLa cells labeled by QD−amPEI-(70K, C16) (scale bars, 200 nm for the left and 100 nm for the right; ER, endoplasmic reticulum; C, cytosol; N, nucleus).

stability and PL properties were maintained for over months at room temperature under ambient atmosphere. The alkyl chains in the PEI backbones are thought to have introduced tight interdigitations with

the hydrophobic surface ligands of QDs, while the outside positively charged hydrophilic part of amPEI well stabilized the colloidal properties.

To tune the HD diameter of QD−amPEI to around 100 nm and also to maximize the PL QE, parameters such as the alkyl chain length, PEI molecular weight (MW), degree of modification (DOM, the percentage of introduced alkyl chains over the entire available amine conjugation sites per PEI), and mixing ratio between the amPEI and QD were studied (see Supporting Information for detail). For optimal parameters, 50% of DOM, mixing molar ratio of 10 between the amPEI and QD were chosen. For comparison of different QD−amPEIs, PEIs of MW 25K or 70K were modified as varying the DOM from zero (unmodified PEIs), 25%, 50%, and to 75% (Supporting Information Figure S5). The mixing ratio between amPEI and QD was varied from 1/10 to 10. When unmodified PEIs were used instead of alkylated amPEIs, the QD composites began to aggregate and showed large HD diameter and small zeta potentials (cases of zero DOM in Supporting Information Figure S5a,b). Similar aggregations were observed when the mixing ratio was 1 or smaller (Supporting Information Figure S5c,d). Within our DOM range between 25 and 75% and mixing ratio between 1/10 and 10, both 25K and 70K PEI showed the smaller HD and larger zeta potential as increasing the DOM or as decreasing the mixing ratio, which plateaued at 50% or higher DOM and at the mixing ratio of 5 or higher. The initial MW of PEI (whether 25K or 70K) showed no meaningful difference when modified and prepared for QD−amPEIs. At the DOM of 50% or higher and at the mixing ratio 5 or higher, the QD−amPEIs typically showed HD ∼100 nm and zeta potential ∼50 mV.

Figure 1a,b shows the TEM images and fluorescence spectrum of a QD−amPEI composite sample prepared from 70K PEI using 50% DOM and the mixing ratio of 10, which is noted as QD−amPEI(70K, C16) (50% DOM and the mixing ratio of 10 were consistently used unless noted otherwise within this manuscript). The TEM images reveal that dozens of QDs were wrapped well by the amPEI. PL spectrum of the QD−amPEI is very similar to that of as-synthesized QD. We have studied the QD cellular labeling efficiencies by different QD−amPEIs along with other conventional QD labeling techniques as the controls. Fourteen different QD samples were prepared: as-synthesized QD, QD−amPEI(70K, C5), QD−amPEI(70K, C8), QD−amPEI(70K, C16), QD−amPEI(25K, C16), QD−amPEI(750K, C16), QD-PEI(25K), QD-PEI(70K), QD-PEI(750K), CTAB-QD (CTAB wrapped as-synthesized QD), Lipo-QD (Lipofectamine wrapped as-synthesized QD), (+)-QD (QD surface-modified by a previously reported ligand which has the dihydrolipoic anchoring unit and tertiary amine functional group on the other end),[25] (−)-QD (QD surface-modified by dihydrolipoic acids), and Lipo-(−)-QD (Lipofectamine wrapped (−)-QD) (see Supporting Information for the preparations of the samples and Figure S6 for schematic representations of the QD samples). PL QE was compared for the 14 samples (Figure 1c). As-synthesized QDs were dispersed in chloroform, and all others were in MES buffer solutions. QD−amPEI(70K, C5), QD−amPEI(70K, C8), QD−amPEI(70K, C16) samples showed the brighter PL as the alkyl chain length increased, presumably because of the enhanced interdigitization interactions with as-synthesized QD surface ligands.[14] QD−amPEI-(70K, C16) in MES buffer showed 84% PL QE of as-synthesized QD in chloroform. All other samples showed the PL QE less than half of QD−amPEI(70K, C16). HD diameter and zeta potential data are also provided for all the 14 samples (Supporting Information Table S1). The 13 samples (besides the as-synthesized QD) were dispersed in aqueous media, and were further cocultured with HeLa cells using 10 nM QD concentration for 2 h. Flow cytometry was performed to quantify the cell labeling efficiency (Figure 1d,e). The 'percentage of labeled cells' is defined as the portion of live cells which exhibit QD PL significantly brighter than autofluorescence level. The 'mean brightness of labeled cells' is the average QD PL intensity of the labeled cells. In the case of QD−amPEI(70K, C5, C8, or C16), the percentage of labeled cells increased for the sample with longer alkyl chains, which suggests that the long alkyl chain accelerates the QD−amPEI cellular uptake presumably by enhanced disruption of multilamellar lipid vesicles.[26] The surfaces of QD−amPEIs may undergo certain rearrangements during endocytosis. The longer alkyl chains, which should mostly face inside, may interact with cellular membranes and facilitate the cellular uptakes. Other samples show comparably high percentages of labeled cells except the cases of CTAB-QD and (−)-QD. The mean brightness of labeled cells showed more dramatic difference between the samples. QD−amPEI(70K, C16) sample showed the prominently strong mean PL, which was followed by QD−amPEI(25K, C16) and QD−amPEI(750K, C16). All other samples showed the mean brightness at the level of one tenth of QD−amPEI(70K, C16) sample. QD−amPEI is expected to adsorb nonspecifically on cell membranes by the electrostatic interaction and disrupt the membrane structures. Cross-sectional TEM studies directly reveal the internalized QD−amPEIs in cells (Figure 1g). The higher mean brightness of QD−amPEI(70K, C16) over QD−amPEI(25K, C16) and QD−amPEI(750K, C16) is thought to originate largely from the fast intracellular delivery kinetics. QD−amPEI(750K, C16) was initially slightly brighter than QD−amPEI(70K, C16), and the percentages of the labeled cells were similar for the two. Surprisingly, mean brightness of QD−amPEI(70K, C16) was more than 5 times larger than that of QD−amPEI(750K, C16). The two QD−amPEIs showed similar HD diameter and

zeta potentials (Supporting Information Table S1). The amphiphilic polymer shell of QD−amPEI(70K) should consist of more number of the amPEI(70K) polymers than the case of QD−amPEI(750K). It is hypothesized that QD−amPEIs with larger number of polymers are more flexible in the shape transformation and also in the rearrangement of surface charge and hydrophobicity distributions. The higher flexibility of QD−amPEI(70K, C16) may have enabled the rapid cellular internalization when compared with QD−amPEI(750K, C16). QD−amPEI(25K, C16) initially showed weaker PL and smaller zeta potential than QD−amPEI(70K, C16), and exhibited notably smaller mean brightness of labeled cells. QD−amPEI(70K, C16) showed the mean brightness of labeled cells, which was more than 10 times brighter than conventional cellular labeling methods such as CTAB-QD, Lipo-QD, (+)-QD, (−)-QD, and Lipo-(−)-QD. For comparison with conventional cellular labeling with fluorescent dyes, the cytometry experiment was repeated using 300 nM of CellTrace (Life Technologies) coculturing with cells. Mean brightness of the fluorescent dye labeled cells showed more than 20 times smaller signal when compared with the case of QD−amPEI(70K, C16) (Supporting Information Figure S7). It is noted that 10 nM concentrations were used for the QD samples while 300 nM was used for CellTrace to match the apparent PL intensities in PBS solutions, which suggests the difference in cellular labeling brightness between the QD−amPEI and CellTrace does not merely originate from a single QD being brighter than a single fluorescent molecule. Such bright QD cellular labeling was achieved by QD−amPEI(70K, C16) by retaining the high QD PL brightness in the transfer process to aqueous phase and also by the efficient intracellular delivery kinetics through the amPEI optimization. The cellular labeling brightness was compared among different QD samples using the autofluorescence level of untreated control cells as the internal reference. The brightness of QD signal in the cells reflects the amount of QD uptake and also the PL QE of the internalized QDs which should be related to the stability within the cells as well. Our QD−amPEI was designed to optimize the two factors: the QD uptake by the cells and the QD brightness/stability within the cells. Optically *z*-axis sectioned microscope images were obtained by confocal microscope for the cocultured HeLa cells with 10 nM QD−amPEI(70K, C16), which confirmed the internalizations of the QD−amPEIs (Supporting Information Figure S8). For QD cellular labeling, minimization of the labeling cytotoxicity is important. Cell viability was quantified after the QD labelings by measuring mitochondrial enzyme activity using the CCK-8 assay for HeLa cells co-incubated with 10 nM QD−amPEI-(70K, C16), QD−amPEI(25K, C16), QD−amPEI(750K, C16), CTAB-QD, Lipo-QD, (+)-QD, (−)-QD, and Lipo-(−)-QD at 12, 24, and 48 h (Figure 1f. Data at 24 h were omitted in Figure 1f for visual clarity and can be found in Supporting Information Figure S9). QD−amPEI(25K, C16) and QD−amPEI(70K, C16) showed no noticeable cytotoxicity up to 48 hours. QD−amPEI(750K, C16) showed considerable toxicity with the viability reduction to half at 48 h. It is well-known that larger MW PEIs show higher cytotoxicity due to severe membrane disruptions.[27] CTAB-QDs showed the most severe cytotoxicity presumably because CTAB molecules can easily detach from bilayers on QDs and disturb the integrity of cell membranes. Lipo-QDs, Lipo-(−)-QDs, (+)-QDs, and (−)-QDs did not show noticeable cytotoxicity, which should be mostly due to the small interaction and internalization to cells.

Our QD−amPEI showed the efficient and bright QD cellular labeling with minimal cytotoxicity. We have further extended the applicability of our QD−amPEIs for simultaneous cellular labeling and gene delivery. PEI is one of the most effective nonviral gene delivery vehicles.[28] Co-delivery of QDs and genes have been reported by others.[29] Bagalkot and co-workers conjugated PEIs to PMAT-encapsulated QDs and used it as siRNA delivery vehicle.[29] Our QD−amPEIs can be an efficient QD and gene co-delivery platform because alkylated PEIs, like our amPEIs, have been reported to show enhanced gene delivery efficiency and lower cytotoxicity.[24] Green fluorescent protein (GFP) silencing siRNA, the 21 base pair double-strand siRNA (see Supporting Information for the siRNA sequence), was loaded onto the outer surface of QD−amPEI(70K, C16) by electrostatic self-assembly. For the GFP silencing siRNA loaded QD−amPEI (QD-amPEI-siRNA), the ratio between the QD−amPEI and siRNA cargo was varied from 10:1 to 1:250 to optimize the gene delivery (Supporting Information Figure S10 for the HD diameter and zeta potential data). The ratio of 1:3 was chosen and used for GFP silencing experiments with GFP expressed Madin Darby canine kidney epithelial cell line (MDCK-GFP cells). Four samples were co-incubated with the MDCK-GFP cells for 4 h: QD−amPEI, QD-amPEI-siRNA, siRNA only (siRNA without gene delivery vehicle), and Lipofectamine-siRNA (siRNA transfection by Lipofectamine) (see Supporting Information for experimental details). Intracellular delivery of QDs and siRNAs by QD-amPEI-siRNA was visualized under fluorescence microscope (Figure 2). Both QD−amPEI and QD-amPEI-siRNA cases showed similar red fluorescence intensities from the internalized QDs, which manifests that the QD-amPEI-siRNA maintains the cellular internalization and QD delivery capability not noticeably compromised by the siRNA loading. QD−amPEI case (with no siRNA) showed comparable GFP green fluorescence as that of untreated control cells, which confirms that the delivery of QD−amPEI does not alter the GFP expression level. Surprisingly, the siRNA gene silencing efficiency was greater for QD-amPEI-siRNA than the case of Lipofectamine-siRNA. The control "siRNA only" showed only slightly

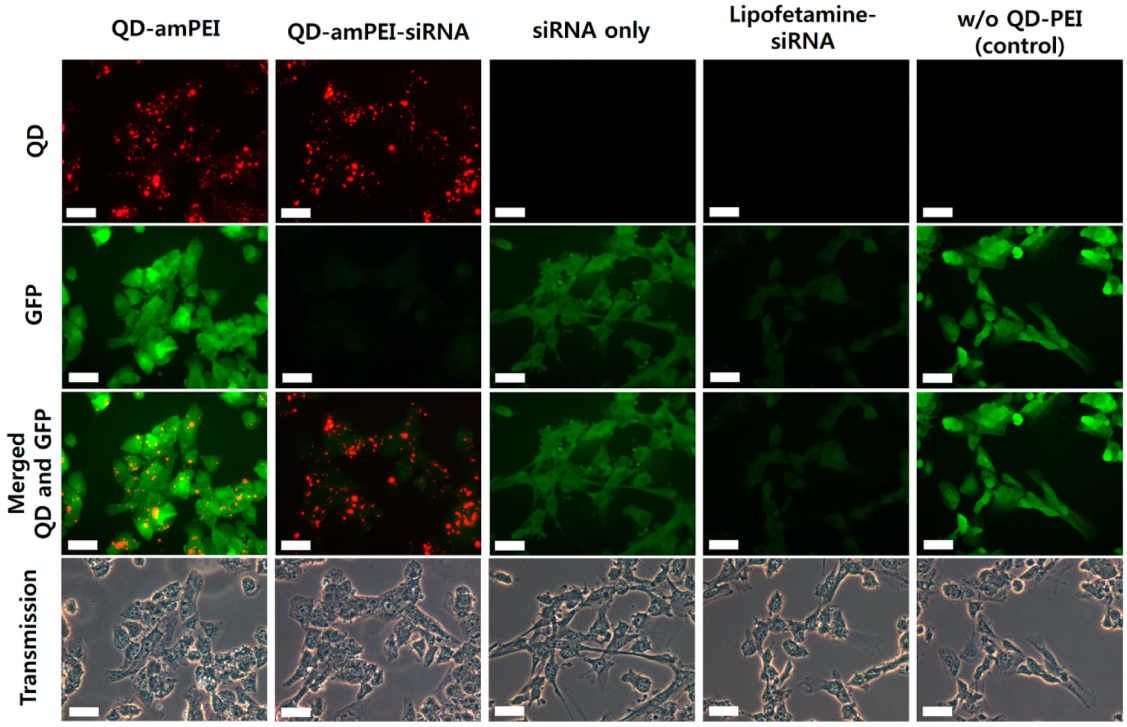

Figure 2. Gene delivery using QD-amPEI-siRNA. Fluorescence microscope images for QD signal (top row), GFP signal (second row), and QD and GFP merged signals (third row). Transmission microscope images (bottom row). MDCK-GFP cells were co-incubated with 10 nM QD−amPEI (first column), 10 nM QD-amPEI-siRNA (second column), 300 nM siRNA (third column), and 1.5 μM Lipofectamine−siRNA complex (fourth column). The control cells were untreated (last column) (scale bars: 50 μm).

dimmer GFP level than the control with no siRNA. For comparison, we lowered the siRNA coculture concentration of QD-amPEI-siRNA to be 9 times smaller than that of Lipofectamine-siRNA case (and the siRNA only case as well). Despite of the smaller siRNA concentration, QD-amPEI-siRNA showed almost double the gene silencing level when compared with Lipofectamine-siRNA. The GFP signal intensity from the QD-amPEI-siRNA case was 56% of that from Lipofectamine-siRNA case. These results demonstrate that our amPEI vehicle allows efficient co-delivery of QDs and siRNAs.

Our amPEI-based platform can be considered as a partitioned vehicle with (i) the inner hydrophobic pocket which is designed to load bright as-synthesized QDs with fatty acids on the QD surfaces and (ii) the outer positively charged surface which allows simple conjugations by electrostatic assemblies. For our QD−amPEI based platform to be useful for various applications, simple endowment of targeting capability is important. For example, targeting capability in conjunction with the QD-amPEI-siRNA will provide a cell-specific gene delivery. To introduce target-specific affinity to QD−amPEIs, HAs were conjugated to QD−amPEIs. HA tethered QD−amPEI (HA-QD-amPEIs) was prepared by electrostatic assemblies through mixing HA (2000 kDa MW) and QD−amPEI(70K, C16) using 100:1 ratio (see Supporting Information Figure S11 for optimization procedures, HD diameter, and zeta potentials for HA-QD-amPEI samples

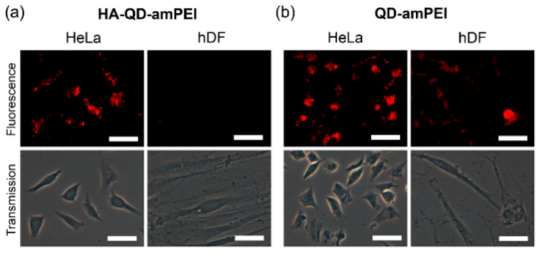

Figure 3. Specific cell targeting by hyaluronic acid conjugated HA-QD-amPEI. Fluorescence and transmission microscope images of HeLa cells (left) and human dermal fibroblast cells (right) that were treated with 50 nM HA-QD-amPEI (a) or with 50 nM QD−amPEI (b) (scale bars: 50 μm).

prepared using different mixing ratios). Overexpression of HA receptor CD44 is known to deeply related to cancer angiogenesis and proliferations. We have previously used HA-conjugated QDs to visualize lymphatic vessels *in vivo*.[30] Human cervical cancer cells, HeLa, were chosen as a CD44 overexpressed group, and human dermal fibroblast cells, Hdf, for the negative control. When co-incubated, HA-QD-amPEIs showed cell-specific labeling for HeLa cells, whereas no noticeable signal could be found for Hdf cells (Figure 3, see Supporting Information for detailed experimental procedures). The specific-to-nonspecific (or HeLa-to-Hdf cell QD signal) fluorescence signal ratio was 120, which demonstrates that our HA-QD-amPEIs can label CD44 overexpressed cell line with marginal nonspecific adsorption on negative cells. On the other hand,

control experiments with QD−amPEIs showed similar QD signals for both HeLa and Hdf cells. These results demonstrate that tethering targeting groups (electrostatic HA conjugation in this case) onto QD−amPEI can achieve high specificity (cell-specificity in this case) without severely perturbing the structural integrity and QD delivery function of QD−amPEI.

Gene delivery and cell-specific labeling have been successfully demonstrated by modifying the outer surface of QD−amPEIs. On the other hand, the inside QD−amPEI compartment can provide a hydrophobic pocket where dozens of QDs and other hydrophobic sensing molecules can interact with each other and thus sense the local microenvironment around the am-PEI based platform. We particularly focused on the possibility that the inside hydrophobic compartment can interact with outside environment because the amPEI based membrane is expected to easily allow permeations of small molecules such as dissolved oxygens. A probe that can monitor in real-time the local oxygen concentration is important to many applications that include studies of tumor growth, metastasis, and proliferation in hypoxic condition and apoptosis by cancer therapy.[31] Spencer and co-workers have reported hypoxic local oxygen concentration of bone marrow using time-resolved PL measurements with platinum(II) porphyrin phosphorescence dye probes.[32] McLaurin and co-workers reported osmium-(II) polypyridyl conjugated QDs for a PL ratiometric oxygen probe.[33] Xu and co-workers have reported silica nanoparticles cohosting tris(4,7-diphenyl-1,10-phenanthroline)ruthenium(II) ($Ru(dpp)_3^{2+}$) phosphorescence oxygen sensing dyes and oxygen insensitive fluorescent Oregon Green dyes that can PL ratiometrically monitor the oxygen concentration.[34] Oxygen sensitive phosphorescence dyes, such as $Ru(dpp)_3^{2+}$, are typically hydrophobic when unmodified. A sub-100 nm hydrophobic pocket that contains both dozens of QDs and dozens of phosphorescence dyes and that can interact with local oxygen molecules is thought to provide an accurate ratiometric PL measurement as averaging the local microenvironmental values. As-synthesized QDs and $Ru(dpp)_3^{2+}$ dye molecules were co-dispersed in chloroform using 1:3 molar ratio, and the mixture solution was used for the preparation of QD and $Ru(dpp)_3^{2+}$ dye cohosting amPEI composite (QD-Ru-amPEI) (see Supporting Information for synthetic details). The QDs act as oxygen insensitive fluorophores that emit at 470 nm (see Supporting Information for the QD preparation) and $Ru(dpp)_3^{2+}$ dye molecules act as an oxygen sensitive phosphore of which emission at 620 nm becomes quenched upon the oxygen binding.[35] QD-Ru-amPEI 100 nM MES buffer solution was placed under ambient air normoxia condition or under hypoxia condition of 100% nitrogen bubbling, and the PL spectra were obtained (Figure 4a). The QD PL was not affected by the conditions; however, the PL intensity of Ru dye increased by 3.0 times from normoxia to hypoxia conditions. Reversibility of the QD-Ru-amPEI was tested by switching the environment between the normoxia and hypoxia conditions for more than 12 cycles (Figure 4b). The QD-Ru-amPEI worked successfully as a reversible ratiometric PL oxygen probe showing the QD and Ru dye PL intensity ratio values between 1.5 and 5.0 (Figure 4b). Oxygen molecules are thought to reversibly permeate in and out of the amPEI scaffold. To accurately calibrate our QD-Ru-amPEI oxygen probe, 10 different oxygen and nitrogen mixture gases were prepared with the compositions ranging from 0 to 100% oxygen and the ratiometric PL values were measured for QD-Ru-amPEI oxygen probes (see Supporting Information for experimental details. See Figure S12 for the calibration curve).

The QD-Ru-amPEI oxygen probe was further applied to cellular environments. HCT116 cells, human colon cancer cells, were co-incubated with 50 nM QD-Ru-amPEI for 4 h, which was followed by the exposure to hypoxic condition using an oxygen-free, serum-free medium or alternatively to normoxic condition using an ambient medium, for additional 4 h (see Supporting Information for experimental details). Under fluorescent microscope, the cells in normoxic condition appear more purple, while the cells in hypoxic condition look more red, which is consistent with the spectra where the hypoxic condition shows prominently stronger red emission from the Ru dyes (Figure 4c). According to the concentration calibration (Supporting Information Figure S12), the normoxic cells were in 20.5(±1.01)% oxygen concentration and 1.10(±0.58)% for hypoxic cells. Cytotoxicity of QD-Ru-amPEI was assayed up to 100 nM concentration for 12 h of co-incubation, where no noticeable toxicity was observed (Supporting Information Figure S13). After the co-incubation with QD-Ru-amPEI and before the exposure to normoxic or hypoxic condition, the cells were carefully washed to remove free QD-Ru-amPEIs. The ratiometric PL signals of QD-Ru-amPEIs should be mostly coming from the intracellular environment. These results show that the QD-Ru-amPEIs can maintain the integrity and the probing function in cells and can act as a sensitive oxygen probe that can be potentially used for subcellular microenvironment.

Inspired by the successful oxygen sensing in cellular level, we have further applied our QD-Ru-amPEIs to tumor spheroid model. Tumor spheroid model is a biological system to study growth and functions of natural 3D tumor mass *in vivo*.[36] Spheroid tumor cells are designed to mimic the growth of invaded tumor cells to another organs. Many molecules can diffuse in and out slowly through the outmost layer of the spheroid cells. The cells in core part of a spheroid are in deficient environment for oxygen and nutrients and thus are almost in necrotic state. Oxygen concentration mapping for spheroid model has been studied by many groups, which includes ratiometric PL based

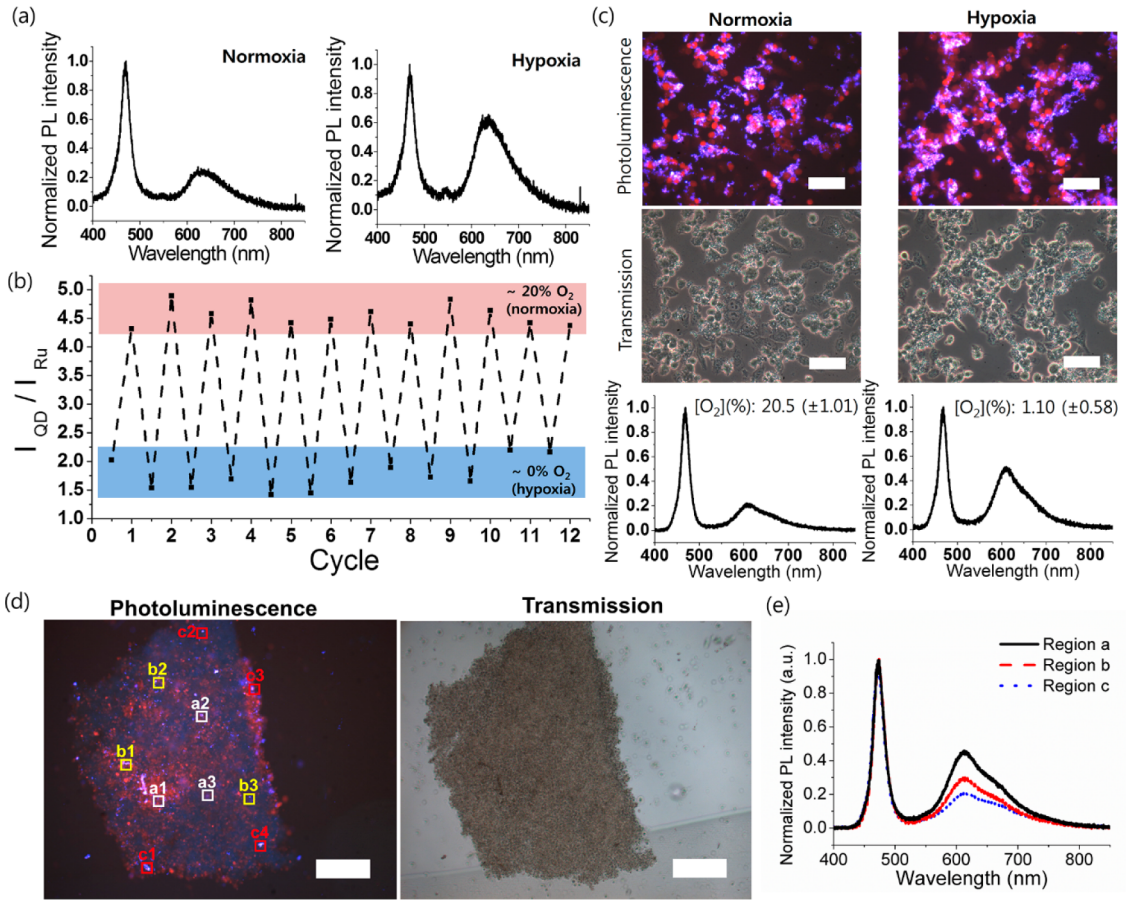

Figure 4. Ratiometric oxygen sensing by QD-Ru-amPEI. (a) PL spectrum of 1 μM QD-Ru-amPEI sample in MES buffer under normoxic (left) and under hypoxic (right) conditions. (b) PL intensity ratio (QD signal to Ru dye signal) values of a QD-Ru-amPEI sample in MES buffer under repeated cycles of normoxic and hypoxic conditions. (c) Fluorescence (top) and transmission (middle) microscope images of HCT116 cells pretreated with QD-Ru-amPEI oxygen probes and subsequently exposed to normoxic (left) or hypoxic (right) condition (scale bars: 50 μm). Emission spectra for the cells under normoxic (bottom left) or hypoxic (bottom right) condition. (d) Photoluminescence and transmission microscope images of spheroid HCT116 cells labeled with 100 nM QD-Ru-amPEIs for 4 h. Different regions of interest were selected from the core region (three white squares of a1, a2, and a3), from the middle region (three yellow squares of b1, b2, and b3), and from the peripheral region (four red squares of c1, c2, c3, and c4) (scale bars: 200 μm). (e) Averaged PL spectra of the regions of interest from the three regions of the core (black solid line), middle (blue dashed line), and peripheral (red dotted line) regions.

mapping using two different dye molecules by Kondrashina and co-workers.[37] Tumor spheroids of hundreds of micrometers were prepared by hanging-drop method (see Supporting Information for experimental details). The spheroid HCT116 cells were co-incubated with 100 nM QD-Ru-amPEIs for 4 h and were observed under fluorescence microscope (Figure 4d). A total of 10 different regions of interest (ROI) were selected in the spheroid cells with three from the core, another three from the middle, and four close to the outmost layer. Averaged fluorescence spectra from the three different regions show the more intense red emission from the Ru dye as the ROI move from the core, middle, to the periphery, whereas no noticeable change for the QD emissions was observed (Figure 4e. See Supporting Information Figure S14 for the entire PL spectra for the 10 ROIs). The averaged oxygen concentrations for the core, middle, and peripheral ROIs were 1.33(±1.01)%, 8.42(±1.26)%, and 19.9(±1.7)%, respectively. The oxygen concentration at the core spheroid ROI is comparable to previously reported values by others: 1.54%[38] (spheroid diameter, ~600 μm) and 2.31%[37] (spheroid diameter, ~300 μm). Hypoxic condition in the spheroid core is known to maintain over 100 μm,[39] which is consistent with our moderately hypoxic condition in the middle ROI of spheroid. The peripheral ROI is ~10 μm apart from the outmost spheroid layer, which allows rapid permeation of oxygen molecules and exhibits normoxic condition. These results demonstrate the potential of our QD-Ru-amPEI oxygen probe for *in vivo* disease animal models which can real-time monitor the tumor microenvironment. Such tumor microenvironment studies can provide new information for tumorigenesis and can be also used for anticancer drug screening.

CONCLUSIONS

In conclusion, we have developed an amPEI-based platform which is ~100 nm in HD diameter and has the

slightly positive outer surface that suites well for cellular internalization. QD−amPEI can efficiently contain dozens of bright as-synthesized QDs inside the hydrophobic pocket. The QD−amPEI was optimized to maximize the intracellular QD delivery by the proper QD cargo size and the rapid endocytosis kinetics. Without any noticeable cytotoxicity, QD−amPEIs were able to label cells with the brightness more than 10 times higher than conventional QD cellular labeling methods such as Lipofectamine-assisted or CTAB-assisted QD labelings. Our QD−amPEI platform has two partitions: positive outer surface and hydrophobic inside pocket. The outer positive surface was further exploited for gene delivery and targeting. QD-amPEI-siRNA has demonstrated the successful co-delivery of QDs and genes. QD-amPEI-siRNA showed the transfection efficiency an order of magnitude higher than conventional gene transfection using Lipofectamine. Targeting HA was tethered in the case of HA-QD-amPEI, which showed the cell-specificity with the PL signal-to-noise ratio over 100. The inside hydrophobic compartment was further applied for cohosting oxygen sensing phosphorescence Ru dyes along with QDs. The QD-Ru-amPEI showed accurate and reversible oxygen sensing capability by the ratiometric PL signals, which was successfully applied to cellular and spheroid models.

METHODS

Synthesis of Amphiphilic Poly(ethylene imine) (amPEI) Polymers. Prior to the alkyl chain conjugation, the 70K polyethyleneimine (PEI) aqueous solution was completely dried out using rotary evaporator at 70 °C and was dispersed in anhydrous chloroform to be 0.1 mM solution (the 70K PEI has approximately 1630 amine functional groups). To the PEI solution, 815 mol equiv of hexadecylisocyanates (for 50% DOM) were added and kept stirred vigorously for 1 h. IR (KBr): $\nu = 1627\ cm^{-1}$ (m, ν (amide C═O)), 1544 cm^{-1} (m, ν (amide N−H)), 3301 cm^{-1} (m, ν (amine N−H)).

Encapsulation of QDs with amPEI (70K, C16)) Polymers and TEM Sample Preparation. The QD hexanes solution prepared by the solvothermal method was purified by precipitation with methanol and redispersion in chloroform. For the 610 nm emitting QDs, the concentration of QD solution was spectrophotometrically determined using the extinction coefficient of $2.26 \times 10^6\ cm^{-1}\ M^{-1}$ at 350 nm. Ten nanomoles of amPEI (70K, C16) polymer solution in chloroform was mixed with 1 nmol of QDs in chloroform. Ten milliliters of MES buffer (100 mM, pH 6.5) was added to the QD and amPEI mixture in chloroform and the solution was sonicated for 30 min. The chloroform in the mixture was removed by vacuum. QD−amPEIs were centrifuged for 20 min at 14 000 rpm 4 °C, and the excess amPEI polymers were removed by decanting. The spun-down QD−amPEIs were readily dispersible in DI water or in buffers for further experiments.

Cell Culture Condition. HeLa cells (human cervical carcinoma cell line) and HCT116 cells (human colon cancer cell line) were maintained in RPMI media (Hyclone) supplemented with 10% (v/v) fetal bovine serum (FBS) and 1% (v/v) penicillin/streptomycin (growth media) for cell adhesion. For further tests on intracellular delivery and cytotoxicity, cell culture medium was changed to serum-free media, which was composed of RPMI media and 1% (v/v) penicillin/streptomycin (serum-free media). MDCK-GFP cells (Mardin-Darby canine kidney cell line, isolated from dog kidney cortex) and Hdf cell (human dermal fibroblast) were maintained in DMEM growth media (Hyclone) for cell adhesion. For further tests on gene delivery or cell-specific labeling, cell culture medium was changed to DMEM serum-free media.

Flow Cytometry Analysis. To investigate the interaction between cells and the QDs, HeLa cells, human cervical carcinoma cells, were cultured with the QD−amPEI composites, (−)-QDs, (+)-QDs, CTAB-QDs, and Lipofectamine-QDs (Lipo-QDs). The cells were grown in RPMI growth media for cell adhesion. Cells were passaged every 5 days and were used within 30 passages. To quantify the nonspecific labeling level of QDs, 5×10^4 HeLa cells were cocultured with the 10 nM of QD−amPEIs or control QD samples for 12 h in serum-free media. For conventional dye-based cellular labeling experiment using commercially available CellTrace Carboxyfluorescein diacetate succinimidyl ester (CFSE) fluorescent dyes, 5×10^4 HeLa cells were cocultured with the 300 nM of CFSE for 12 h in serum-free media. The cells were detached by adding a 0.25% trypsin and EDTA solution. The cells were then rinsed with PBS buffer (0.1 M, pH 7.4) with 1% FBS (FACS buffer) for three times and redispersed in fixing buffer (1% formaldehyde in FACS buffer). The collected cells were further analyzed with flow cytometry.

Cross-Sectional TEM Measurements. HeLa cells were incubated with 10 nM QD−amPEI(70K, C16) in RPMI serum-free media for 12 h. For visualization through TEM, cells were fixed with 2.5% glutaraldehyde in cacodylate buffer (0.1 M, pH 7.2) for 24 h at 4 °C and rinsed with cold (4 °C) cacodylate buffer (0.1 M, pH 7.2) three times again. The cells were dehydrated by series of graded ethanol (50%, 60%, 70%, 80%, 90%, 95%, 98%, and 100%) and propylene oxide and finally embedded with epoxy resin (Epon 812). The samples were then polymerized at 60 °C for 24 h, cut into thin slices using an ultramicrotome (Leica), and collected on 200-mesh copper grids. The thin sections were stained with uranyl acetate (2% in ethanol) for 10 min and lead citrate for 5 min and observed on a Philips Tecnai G2 F20 transmission electron microscope at 200 kV.

Conflict of Interest: The authors declare no competing financial interest.

Acknowledgment. This research was supported by the Bio & Medical Technology Development Program of the National Research Foundation (NRF) funded by the Korean government (MEST) (No. 2011-0019635), a grant from the National R&D Program for Cancer Control, Ministry for Health and Welfare, Republic of Korea (1320220), Engineering Research Center grant (No. 2011-0030075) of the National Research Foundation (NRF), a grant of the Korea Health Technology R&D Project through the Korea Health Industry Development Institute (KHIDI), funded by the Ministry of Health & Welfare, Republic of Korea (HI12C1642), and International Research & Development Program of the NRF funded by the Ministry of Science, ICT and Future Planning (MSIP) of Korea (NRF-2014K1A3A1A49070433).

Supporting Information Available: Details of experimental procedures, FT-IR characterizations for amPEI synthesis, PL spectrum and TEM images of as-synthesized QDs, HD diameter and zeta potential values of different QD−amPEIs prepared for optimizations for cellular labeling, *z*-axis sectioned confocal images of HeLa cells labeled with QD−amPEI(70K, C16), additional cytotoxicity data, HD diameter and zeta potential values of QD-amPEI-siRNAs and HA-QD-amPEIs, a calibration plot for QD-Ru-amPEI ratiometric signal *vs* oxygen concentration, cell viabilities of HCT116 cells treated by QD-Ru-amPEIs, and raw PL spectra for the entire regions of interest in spheroid HCT116 cells. The Supporting Information is available free of charge on the ACS Publications website at DOI: 10.1021/acsnano.5b02357.

REFERENCES AND NOTES

1. Chan, W. C. W.; Maxwell, D. J.; Gao, X.; Bailey, R. E.; Han, M.; Nie, S. Luminescent Quantum Dots for Multiplexed Biological Detection and Imaging. *Curr. Opin. Biotechnol.* **2002**, *13*, 40–46.

2. Medintz, I. L.; Uyeda, H. T.; Goldman, E. R.; Mattoussi, H. Quantum Dot Bioconjugates for Imaging, Labelling and Sensing. *Nat. Mater.* **2005**, *4*, 435–446.
3. Mattoussi, H.; Palui, G.; Na, H. B. Luminescent Quantum Dots as Platforms for Probing *in Vitro* and *in Vivo* Biological Processes. *Adv. Drug Delivery Rev.* **2012**, *64*, 138–166.
4. Unger, R. H.; Zhou, Y.-T.; Orci, L. Regulation of Fatty Acid Homeostasis in Cells: Novel Role of Leptin. *Proc. Natl. Acad. Sci. U.S.A.* **1999**, *96*, 2327–2332.
5. Dubertret, B.; Skourides, P.; Norris, D. J.; Noireaux, V.; Brivanlou, A. H.; Libchaber, A. *In Vivo* Imaging of Quantum Dots Encapsulated in Phospholipid Micelles. *Science* **2002**, *298*, 1759–1762.
6. Hu, X.; Gao, X. Silica−Polymer Dual Layer-Encapsulated Quantum Dots with Remarkable Stability. *ACS Nano* **2010**, *4*, 6080–6086.
7. Valencia, P. M.; Basto, P. A.; Zhang, L.; Rhee, M.; Langer, R.; Farokhzad, O. C.; Karnik, R. Single-Step Assembly of Homogenous Lipid−Polymeric and Lipid−Quantum Dot Nanoparticles Enabled by Microfluidic Rapid Mixing. *ACS Nano* **2010**, *4*, 1671–1679.
8. Pellegrino, T.; Manna, L.; Kudera, S.; Liedl, T.; Koktysh, D.; Rogach, A. L.; Keller, S.; Rädler, J.; Natile, G.; Parak, W. J. Hydrophobic Nanocrystals Coated with an Amphiphilic Polymer Shell: A General Route to Water Soluble Nanocrystals. *Nano Lett.* **2004**, *4*, 703–707.
9. Geidel, C.; Schmachtel, S.; Riedinger, A.; Pfeiffer, C.; Müllen, K.; Klapper, M.; Parak, W. J. A General Synthetic Approach for Obtaining Cationic and Anionic Inorganic Nanoparticles *via* Encapsulation in Amphiphilic Copolymers. *Small* **2011**, *7*, 2929–2934.
10. Yu, W. W.; Chang, E.; Falkner, J. C.; Zhang, J.; Al-Somali, A. M.; Sayes, C. M.; Johns, J.; Drezek, R.; Colvin, V. L. Forming Biocompatible and Nonaggregated Nanocrystals in Water Using Amphiphilic Polymers. *J. Am. Chem. Soc.* **2007**, *129*, 2871–2879.
11. Gao, X.; Cui, Y.; Levenson, R. M.; Chung, L. W. K.; Nie, S. *In Vivo* Cancer Targeting and Imaging with Semiconductor Quantum Dots. *Nat. Biotechnol.* **2004**, *22*, 969–976.
12. Lees, E. E.; Nguyen, T.-L.; Clayton, A. H. A.; Mulvaney, P. The Preparation of Colloidally Stable, Water-Soluble, Biocompatible, Semiconductor Nanocrystals with a Small Hydrodynamic Diameter. *ACS Nano* **2009**, *3*, 1121–1128.
13. Luccardini, C.; Tribet, C.; Vial, F.; Marchi-Artzner, V.; Dahan, M. Size, Charge, and Interactions with Giant Lipid Vesicles of Quantum Dots Coated with an Amphiphilic Macromolecule. *Langmuir* **2006**, *22*, 2304–2310.
14. Anderson, R. E.; Chan, W. C. W. Systematic Investigation of Preparing Biocompatible, Single, and Small ZnS-Capped CdSe Quantum Dots with Amphiphilic Polymers. *ACS Nano* **2008**, *2*, 1341–1352.
15. Ostermann, J.; Merkl, J.-P.; Flessau, S.; Wolter, C.; Kornowksi, A.; Schmidtke, C.; Pietsch, A.; Kloust, H.; Feld, A.; Weller, H. Controlling the Physical and Biological Properties of Highly Fluorescent Aqueous Quantum Dots Using Block Copolymers of Different Size and Shape. *ACS Nano* **2013**, *7*, 9156–9167.
16. Sun, T.; Li, K.; Li, Y.; Li, C.; Zhao, W.; Chen, L.; Chang, Y. Optimizing Conditions for Encapsulation of QDs by Varying PEG Chain Density of Amphiphilic Centipede-Like Copolymer Coating and Exploration of QDs Probes for Tumor Cell Targeting and Tracking. *New J. Chem.* **2012**, *36*, 2383–2391.
17. Cortesi, R.; Esposito, E.; Menegatti, E.; Gambari, R.; Nastruzzi, C. Effect of Cationic Liposome Composition on *in Vitro* Cytotoxicity and Protective Effect on Carried DNA. *Int. J. Pharm.* **1996**, *139*, 69–78.
18. Xu, D.-M.; Yao, S.-D.; Liu, Y.-B.; Sheng, K.-L.; Hong, J.; Gong, P.-J.; Dong, L. Size-Dependent Properties of M-PEIs Nanogels for Gene Delivery in Cancer Cells. *Int. J. Pharm.* **2007**, *338*, 291–296.
19. Chithrani, B. D.; Ghazani, A. A.; Chan, W. C. W. Determining the Size and Shape Dependence of Gold Nanoparticle Uptake into Mammalian Cells. *Nano Lett.* **2006**, *6*, 662–668.
20. Zhang, S.; Li, J.; Lykotrafitis, G.; Bao, G.; Suresh, S. Size-Dependent Endocytosis of Nanoparticles. *Adv. Mater.* **2009**, *21*, 419–424.
21. Boussif, O.; Lezoualc'h, F.; Zanta, M. A.; Mergny, M. D.; Scherman, D.; Demeneix, B.; Behr, J. P. A Versatile Vector for Gene and Oligonucleotide Transfer into Cells in Culture and *in Vivo*: Polyethylenimine. *Proc. Natl. Acad. Sci. U.S.A.* **1995**, *92*, 7297–7301.
22. Nann, T. Phase-Transfer of CdSe@ZnS Quantum Dots using Amphiphilic Hyperbranched Polyethylenimine. *Chem. Commun.* **2005**, *13*, 1735–1736.
23. Duan, H.; Nie, S. Cell-Penetrating Quantum Dots Based on Multivalent and Endosome-Disrupting Surface Coatings. *J. Am. Chem. Soc.* **2007**, *129*, 3333–3338.
24. Thomas, M.; Klibanov, A. M. Enhancing Polyethylenimine's Delivery of Plasmid DNA into Mammalian Cells. *Proc. Natl. Acad. Sci. U.S.A.* **2002**, *99*, 14640–14645.
25. Park, J.; Nam, J.; Won, N.; Jin, H.; Jung, S.; Jung, S.; Cho, S.-H.; Kim, S. Compact and Stable Quantum Dots with Positive, Negative, or Zwitterionic Surface: Specific Cell Interactions and Non-Specific Adsorptions by the Surface Charges. *Adv. Funct. Mater.* **2011**, *21*, 1558–1566.
26. Takigawa, D. Y.; Tirrell, D. A. Interactions of Synthetic Polymers with Cell Membranes and Model Membrane Systems. Part 6. Disruption of Phospholipid Packing by Branched Poly(ethylenimine) Derivatives. *Macromolecules* **1985**, *18*, 338–342.
27. Fischer, D.; Bieber, T.; Li, Y.; Elsässer, H.-P.; Kissel, T. A Novel Non-Viral Vector for DNA Delivery Based on Low Molecular Weight, Branched Polyethylenimine: Effect of Molecular Weight on Transfection Efficiency and Cytotoxicity. *Pharm. Res.* **1999**, *16*, 1273–1279.
28. Parker, A. L.; Newman, C.; Briggs, S.; Seymour, L.; Sheridan, P. J. Nonviral Gene Delivery: Techniques and Implications for Molecular Medicine. *Expert Rev. Mol. Med.* **2003**, *5*, 1–15.
29. Bagalkot, V.; Gao, X. siRNA-Aptamer Chimeras on Nanoparticles: Preserving Targeting Functionality for Effective Gene Silencing. *ACS Nano* **2011**, *5*, 8131–8139.
30. Bhang, S. H.; Won, N.; Lee, T.-J.; Jin, H.; Nam, J.; Park, J.; Chung, H.; Park, H.-S.; Sung, Y.-E.; Hahn, S. K.; et al. Hyaluronic Acid−Quantum Dot Conjugates for *in Vivo* Lymphatic Vessel Imaging. *ACS Nano* **2009**, *3*, 1389–1398.
31. Harris, A. L. Hypoxia—A Key Regulatory Factor in Tumour Growth. *Nat. Rev. Cancer* **2002**, *2*, 38–47.
32. Spencer, J. A.; Ferraro, F.; Roussakis, E.; Klein, A.; Wu, J.; Runnels, J. M.; Zaher, W.; Mortensen, L. J.; Alt, C.; Turcotte, R.; et al. Direct Measurement of Local Oxygen Concentration in the Bone Marrow of Live Animals. *Nature* **2014**, *508*, 269–273.
33. McLaurin, E. J.; Greytak, A. B.; Bawendi, M. G.; Nocera, D. G. Two-Photon Absorbing Nanocrystal Sensors for Ratiometric Detection of Oxygen. *J. Am. Chem. Soc.* **2009**, *131*, 12994–13001.
34. Xu, H.; Aylott, J. W.; Kopelman, R.; Miller, T. J.; Philbert, M. A. A Real-Time Ratiometric Method for the Determination of Molecular Oxygen Inside Living Cells Using Sol−Gel-Based Spherical Optical Nanosensors with Applications to Rat C6 Glioma. *Anal. Chem.* **2001**, *73*, 4124–4133.
35. Coogan, M. P.; Court, J. B.; Gray, V. L.; Hayes, A. J.; Lloyd, S. H.; Millet, C. O.; Pope, S. J. A.; Lloyd, D. Probing Intracellular Oxygen by Quenched Phosphorescence Lifetimes of Nanoparticles Containing Polyacrylamide-Embedded $[Ru(dpp(SO_3Na)_2)_3]Cl_2$. *Photochem. Photobiol. Sci.* **2010**, *9*, 103–109.
36. Sutherland, R. Cell and Environment Interactions in Tumor Microregions: The Multicell Spheroid Model. *Science* **1988**, *240*, 177–184.
37. Kondrashina, A. V.; Dmitriev, R. I.; Borisov, S. M.; Klimant, I.; O'Brien, I.; Nolan, Y. M.; Zhdanov, A. V.; Papkovsky, D. B. A Phosphorescent Nanoparticle-Based Probe for Sensing and Imaging of (Intra)Cellular Oxygen in Multiple Detection Modalities. *Adv. Funct. Mater.* **2012**, *22*, 4931–4939.

38. Dmitriev, R. I.; Zhdanov, A. V.; Nolan, Y. M.; Papkovsky, D. B. Imaging of Neurosphere Oxygenation with Phosphorescent Probes. *Biomaterials* **2013**, *34*, 9307–9317.
39. Glicklis, R.; Merchuk, J. C.; Cohen, S. Modeling Mass Transfer in Hepatocyte Spheroids *via* Cell Viability, Spheroid size, and Hepatocellular Functions. *Biotechnol. Bioeng.* **2004**, *86*, 672–680.